



Cite this: DOI: 10.1039/c5nj02865e

Potential of templated mesoporous aluminas as supports for HDS CoMo catalysts

 Andres Miño,^a Christine Lancelot,^{†*a} Pascal Blanchard,^a Carole Lamonier,^a
Loïc Rouleau,^b Magalie Roy-Auberger,^b Sébastien Royer^{*ac} and Edmond Payen^a

Aluminas, exhibiting different textural properties, were prepared using a template assisted sol–gel method. In the presence of a triblock copolymer as a porogen, and owing to the control of the synthesis parameters, alumina textural properties can be adjusted up to values higher than those of conventional alumina. Among obtained supports, some were selected in order to cover surface area values from 350 to 450 m² g⁻¹, and pore diameters from 5.4 to 9.0 nm. CoMo derived catalysts, prepared by impregnation with a (Co₂Mo₁₀O₃₈H₄)Co₃ solution, with a concentration corresponding to a molybdenum density of 4 atMo nm⁻² (or 3 when not possible to achieve 4), exhibit decreased textural parameters. However, despite the changes induced by the preparation step, the final catalysts always display attractive textural properties. Activities in thiophene hydrodesulfurization (HDS) can be increased by a factor three, depending on the textural properties of the supports used and possibly to some extent on the residual carbon content in the material. The performance of the most efficient solid in the HDS of thiophene was evaluated in the HDS of a straight run gas oil (SRGO) and was found higher than that of a commercial alumina based catalyst and close to that of a commercial catalyst modified by a chelating agent, evaluated under the same conditions.

 Received (in Nottingham, UK)
15th October 2015,
Accepted 20th January 2016

DOI: 10.1039/c5nj02865e

www.rsc.org/njc

1. Introduction

The constant evolution of sulfur content regulations in transportation fuels, toward lower concentrations, imposes a drastic improvement of the hydrodesulfurization (HDS) of petroleum feedstock which can be achieved through the development of more efficient catalytic formulations.¹ Conventional HDS catalysts are composed of nanometric MoS₂ crystallites, promoted by cobalt atoms, dispersed on alumina (CoMo-S phase).^{2–4} This active phase is obtained by the sulfidation of an oxidic precursor generally prepared by incipient wetness impregnation of the precursors (*e.g.* cobalt nitrate and ammonium heptamolybdate) on a porous support.⁵ Textural parameters of the support, *i.e.* specific surface area (SSA) and pore volume (V_p), are parameters conditioning dispersion of the active precursors. A high surface area is needed to achieve high active phase dispersion while a

large pore volume allows the impregnation of high metal loadings.^{6,7} In addition, large pore diameters (D_p) ensure an efficient diffusion of the reactants to the active sites, an issue of particular importance for the treatment of heavy feedstocks.⁸

In this context, the development of alumina supports with improved textural properties is of prime interest. In line with the first reports on the synthesis of mesostructured silica,⁹ many templating strategies were proposed for alumina.^{10–13} The first preparation of templated alumina, in 1996, was proposed using a non-ionic template assisted sol–gel approach.¹⁰ Using a Tergicol-type template, alumina with a surface area higher than 500 m² g⁻¹ can be produced with the pore size in the mesopore domain. At the same time, Vaudry *et al.* proposed the synthesis of alumina in the presence of carboxylic acids.¹¹ Parameters such as the amount of water, the type of solvent, the calcination temperature and the nature of the structuring agent (from different carboxylic acids) significantly impact the textural properties of the final material. After calcination at moderate temperature, *e.g.* 400 °C, alumina exhibiting a surface area up to 700 m² g⁻¹ with narrow pore size distribution in the low mesopore domain size (~2 nm) was obtained.

Until now, non-ionic templating agents have been mostly used in order to produce porous aluminas exhibiting improved surface areas and relatively large pores (Table 1). Prepared using a template assisted sol–gel synthesis route, alumina with surface areas higher than 400 m² g⁻¹ can be easily obtained

^a Univ. Lille, CNRS, Centrale Lille, ENSCL, Univ. Artois, UMR 8181-UCCS-Unité de Catalyse et Chimie du Solide, F-59000 Lille, France.

E-mail: christine.lancelot@univ-lille1.fr

^b IFP Energies Nouvelles, Rond-Point de l'Echangeur de Solaize, BP3, 69360 Solaize, France

^c Université de Poitiers, CNRS IC2MP UMR 7285, 4 Rue Michel Brunet, 86022

Poitiers Cedex, France. E-mail: sebastien.royer@univ-poitiers.fr

[†] Unité de Catalyse et de Chimie de Solide, UMR CNRS 8181, Université Lille 1, bâtiment C3, 59655 Villeneuve d'Ascq, France. Fax: (+33) 3 20 43 65 61; Tel: (+33) 3 20 43 49 50

after calcination at a temperature compatible with the hydro-treatment process (that is between 400 and 600 °C). Even at such high surfaces, the mesopore size could be stabilized, from 2–3 nm (small mesopores) to 10 nm and higher (large mesopores adequate for catalytic treatment of heavy charges). Ordered alumina is however rarely obtained, except using an Evaporation Induced Self-Assembly [EISA] process^{14–16} and most of the materials have vermicular porous structures, demonstrating a lower level of organization compared to that obtained with silica.

While mesostructured silica-based materials were extensively studied as HDS catalyst supports,^{22–32} the literature concerning the use of non-siliceous mesostructured oxides for HDS reactions is in contrast relatively limited. A high capacity for molybdenum dispersion was however reported by Čejka *et al.*³³ and Kaluža *et al.*³⁴ over these mesoporous aluminas. Adequately dispersed molybdenum species were identified on these supports, even at MoO₃ loading as high as 30 wt%, while the formation of bulk phases is evidenced from 16 wt% MoO₃ loading over classical aluminas.³⁵ On mesoporous supported CoMo-S catalysts, Bejenaru *et al.*³⁶ showed that the material HDS activity (as evaluated for the thiophene desulfurization) varies over a wide range, depending on the initial support morphology and its stability upon the impregnation–calcination–sulfidation steps. The best performances were obtained using alumina support presenting a fine fibrillary type morphology with large mesopores. HDS performances of the catalytic materials also depend on the nature of the molybdate species present in the oxidic form on the support surface. Low activity was paralleled to the formation of oxidic monomolybdate species, whereas polymolybdate species, identified before sulfidation, ensured higher activity for the final materials. Badoga *et al.*³⁷ prepared NiMo catalysts supported on mesoporous alumina obtained by the hydrolysis of aluminum isopropoxide

in the presence of P123. For their selected application, that are HDS and HDN (hydrodenitrogenation) of heavy gas oil, they related the improved performance measured for these materials to a higher reducibility of molybdenum when supported over these materials. The limited amounts of the available literature however show the real potential of mesostructured alumina as support for HDS catalysts, especially when the petroleum cuts to be treated correspond to the medium to high distillation temperature ranges.

In this work, starting from the approach proposed by Zhang and Pinnavaia¹⁷ consisting of a copolymer triblock templating sol-gel derived synthesis, aluminas having different textural properties were prepared. The study of the synthesis parameters allowed us to adjust the final textural properties of the supports, which were further used for the dispersion of cobalt and molybdenum precursors. Catalysts (and supports when relevant) were characterized to evaluate the impact of the support characteristics on the thiophene HDS performance of the final CoMo based materials.

2. Experimental

2.1. Alumina synthesis

Alumina preparation presented in this study consists of a template assisted sol-gel synthesis, as initially proposed by Zhang and Pinnavaia (Table 1).¹⁷ Chemicals for the synthesis are used as received: Pluronic P123 (Aldrich, poly(ethylene glycol)-*block*-poly(propylene glycol)-*block*-poly(ethylene glycol), EO₂₀PO₇₀EO₂₀), aluminum-*sec*-butoxide (Aldrich, 97%) as the aluminum source, and 1-butanol (Aldrich, 99.5%+) as the solvent. The molar composition of the initial solution is

Table 1 Selected reference studies for the production of high surface area mesoporous alumina supports

	Synthesis approach	Thermal treatment	Main characteristics of final materials
Zhang and Pinnavaia ¹⁷	MSU-X aluminas prepared using a template (Tergicol and Pluronic) derived sol-gel route, with the insertion of Ce/La for thermal stability improvement	From 500 °C to 600 °C	Amorphous materials, with SSA from 350 to 530 m ² g ⁻¹ , <i>D_p</i> from 5.0 to 10.8 nm and <i>V_p</i> from 0.3 to 1.3 cm ³ g ⁻¹ – wormhole-like porosity
Pinnavaia <i>et al.</i> ¹⁸	Review the different approach for the preparation of amorphous/crystalline mesoporous alumina, using various surfactants. Propose the preparation of mesoporous γ -type alumina, from the boehmite precursor. A crystalline AlOOH precursor can be obtained by the hydrothermal treatment of the amorphous precursor in the presence of the template.		
Čejka <i>et al.</i> ¹⁹	Preparation of mesoporous alumina, using stearic acid as a surfactant, with intermediate hydrothermal treatment being applied. Thermal treatment at intermediate to high temperatures to evaluate textural stabilities	From 420 °C to 1000 °C	Amorphous–crystalline materials (depends on calcination T), with SSA from 480 to 140 m ² g ⁻¹ , <i>D_p</i> from 3.4 to 6.0 nm and <i>V_p</i> from 0.53 to 0.28 cm ³ g ⁻¹ – wormhole-like porosity
Niesz <i>et al.</i> ²⁰	Evaporation induced self-assembly of a hybrid precursor, starting from an organic aluminum precursor in HCl acidified ethanol solution and the Pluronic type template. Calcination at intermediate temperature to ensure the combustion of the copolymer template	400 °C	SSA from 206 to 410 m ² g ⁻¹ , <i>D_p</i> from 3.9 to 6.7 nm and <i>V_p</i> from 0.44 to 0.80 cm ³ g ⁻¹ – from the hexagonal-type pore structure (low H ₂ O content) to wormhole-like porosity (larger H ₂ O content)
Caragheorghieopol <i>et al.</i> ²¹	Two approaches for the preparation of Pluronic and Tergicol templated aluminas: (i) precipitation by ammonia of an organic aluminum precursor and (ii) hydrolysis of an organic aluminum precursor in anhydrous alcohol	540 °C	SSA from 270 to 450 m ² g ⁻¹ , <i>D_p</i> from 4.3 to 8.9 nm and <i>V_p</i> from 0.53 to 1.36 cm ³ g ⁻¹

1 Al: x P123:15ButOH: y H₂O (where $x = 0, 0.2, 0.3, 0.6$ mol, and $y = 2.9, 4.5, 5.9$). An adequate mass of P123 is initially dissolved in 1-butanol at a temperature of 35 °C under mechanical stirring at 400 rpm. After complete dissolution of the template, the hydrolysis temperature is adjusted to z °C ($z = 15, 25, 50$ °C). The aluminum precursor is then added dropwise, and the mixture is stirred at 400 rpm for 1 h. The hydrolysis step is carried out by the dropwise addition of a butanol/water solution ($V_{\text{ButOH}}/V_{\text{H}_2\text{O}} = 1$) at the desired z °C temperature. The solution is aged under stirring for 4 h. The gel is thereafter transferred into a Teflon-lined autoclave and thermally treated at w °C ($w = 15, 45, 65, 85$ °C) for 40 h under static conditions. After thermal treatment, the product is recovered by filtration, washed with butanol, and then dried at 60 °C for 24 h. Finally, the dried solid is calcined under air at 600 °C for 4 h (temperature increase rate = 1 °C min⁻¹), a temperature sufficient to ensure the removal of organic matter from the solid. The nomenclature of the alumina support is as follows: Al-S x -W y -Th z -HT w , where S x refers to the surfactant content, W y to the water content, Th z to the temperature of hydrolysis and HT w to the hydrothermal treatment temperature.

2.2. Catalyst preparation

Supported CoMo oxidic precursors were prepared by incipient wetness impregnation, with an aqueous solution of Co₂Mo₁₀O₃₈H₄Co₃ salt synthesized according to ref. 38, which will be named Co₂Mo₁₀ hereafter. Concentration is calculated taking into account a final molybdenum density of 4 atMo nm⁻² on the final materials, except otherwise specified. The Co/Mo molar ratio, imposed by the stoichiometry of the heteropoly-compound, is 0.5. Impregnation is performed by the dropwise addition of the solution, followed by 2 h of maturation under a wet atmosphere in order to ensure a complete filling of the pores by the impregnation solution. Thereafter, the solids are dried overnight at 100 °C, before being calcined at 500 °C under oxygen. Catalysts are named CoMo x /Al- y , with x being the molybdenum content in wt% of MoO₃, and y the selected alumina.

2.3. Physical characterization

N₂ adsorption-desorption isotherms were recorded at -196 °C using an automated ASAP2010 instrument from MICROMERITICS. Before each run, a known mass of the sample (around 0.200 g) was heated at 350 °C under vacuum for 3 h. Specific surface areas were calculated from the linear part of the Brunauer-Emmett-Teller line. Pore size distributions were obtained by applying the Barrett-Joyner-Halenda (BJH) equation to the desorption branch of the isotherm. The total pore volume was estimated from the N₂ uptake at a P/P_0 value corresponding to the top of the condensation capillary step: 0.99 for solids presenting type IV isotherms, 0.80 for Al-A solids and 0.95 for solids Al-E and Al-F.

Catalysts in their oxidic form were characterized using X-ray photoelectron spectroscopy (XPS). The powdered samples were pressed into an indium foil attached to the sample holder. XPS spectra were recorded using a VG ESCALAB 220 XL spectrometer equipped with a monochromatic Al K α ($E = 1486.6$ eV)

X-ray source. The binding energies were referred to the Al2p photopeak of the support at 74.6 eV. The surface atomic ratios were calculated using the CASA XPS software after subtracting the nonlinear Shirley background.

Dispersion of the oxomolybdate phase over the support was evaluated using Raman spectroscopy. Spectra were recorded at room temperature using a Raman microprobe Infinity from Jobin-Yvon, equipped with a N₂ cooled CCD detector. The exciting laser source was the 532 nm line of a Nd-YAG laser.

2.4. Thiophene catalytic test

HDS of thiophene is commonly admitted as a reference HDS catalytic test, as thiophene is the simplest molecule representative of the aromatic sulfur compounds present in the feeds to be treated.³⁹ Also, HDS of thiophene was selected since this reaction is known to efficiently probe the dispersion of the active phase of HDS catalysts, and will thus allow a first comparison between the solids. The tests were performed at atmospheric pressure in a flow-type reactor packed with 0.2 g of catalyst. Before reaction, the oxidic catalyst was sulfided at atmospheric pressure under a flow of 10 vol% of H₂S in H₂ (100 mL min⁻¹), at 400 °C for 2 h (temperature increase rate of 6 °C min⁻¹). The reactor was then naturally cooled down to the reaction temperature of 300 °C under sulfidation flow. Thiophene, previously purified by two successive vacuum distillations, was introduced in the reactor at a constant pressure of 6.65 kPa in a flow of hydrogen (total flow rate = 10 mL min⁻¹). Reactants and products (butane, but-1-ene, *trans*-but-2-ene, and *cis*-but-2-ene) were analyzed using a gas chromatograph equipped with a flame ionization detector and a Plot-alumina column. Taking into account the relative response factor for each compound, the conversion α was calculated using eqn (1).

$$\alpha = \frac{\sum_{i=1}^4 \frac{a_i}{4}}{\frac{a_{\text{thio}}}{3.4} + \sum_{i=1}^4 \frac{a_i}{4}} \quad (1)$$

where a_i is the peak area corresponding to the i product and a_{thio} is the area of the peak of thiophene.

Values of conversion are reported after four hours of catalyst activity stabilization.

2.5. Straight run gas oil (SRGO) HDS activity

The efficiency of the catalysts towards more refractory molecules was evaluated through the HDS of a gas oil, a real feedstock, instead of using model molecules such as those classically used (like HDS of DBT). Two catalysts were tested using a high pressure up-flow microreactor. Prior to testing the solids were shaped in pellets (size between 0.3 and 0.5 mm). For each test 10 mL of catalyst pellets diluted with 15 mL of carborundum (0.25 mm) were loaded in the isothermal zone of the reactor. The catalysts were sulfided using a mixture of dimethyldisulfide (DMDS) and SRGO containing 1 wt% S (2 wt% DMDS + SRGO) and H₂. After sulfidation, the feed was switched to the test feed (the same SRGO as for sulfidation), the operating conditions

being as follows: pressure = 35 bar; $H_2/oil = 250$ NL/L; LHSV = 2 h^{-1} . During each run, the temperature was changed in the sequence 350–360–370 °C. The total sulfur contents of feed and product samples were determined using an Antek 9000S sulfur analyzer (Ultra-Violet fluorescence).

3. Results and discussion

Synthesis parameters were varied during the preparation of the alumina supports, such as the quantity of porogen, the quantity of water for the hydrolysis step, the hydrolysis temperature and the autoclaving temperature (solids Al-A to Al-K). Among the prepared supports, 6 aluminas were then selected to be used as HDS CoMo catalyst supports, on the basis of their textural parameters. Surface areas, porous volumes and pore diameters of the alumina and of the corresponding catalysts are listed in Table 2, as well as the maximum molybdenum densities imposed by the water pore volume of the solids (corresponding to the amount of water necessary to wet the support without excess). Among the selected supports, two cannot achieve the desired dMo of $4\text{ at}_{Mo}\text{ nm}^{-2}$ due to their low porous volume, but were however chosen due to their high SSA (Al-B and Al-I). The corresponding catalysts were then prepared at a molybdenum density of $3\text{ at}_{Mo}\text{ nm}^{-2}$. The dMo achieved on the final solid (dMo_{real}) is calculated taking into account the variation of the surface area of the support during the impregnation–calcination process. For comparison purposes, a commercial alumina, the Pural SB3 noted Al-P, was also used for catalyst preparation, with a dMo of $4\text{ at}_{Mo}\text{ nm}^{-2}$.

3.1. Characterization of aluminas synthesized by the sol-gel method in the presence of P123

Effect of structuring agents, A–B–C–D aluminas in Table 2. In samples Al-A, Al-B, Al-C and Al-D, porogen content was varied from 0 to 0.6 mole per mole of Al^{3+} in the synthesis

gel. When comparing with solid Al-A prepared without porogen, the addition of 0.2 mole of P123 allows obtaining a solid with higher SSA (+24% for Al-B). An increase in pore volume and in pore diameter is also observed, +25% and +11%, respectively. When still increasing the porogen content, SSA decreases from $445\text{ m}^2\text{ g}^{-1}$ for the Al-B solid to $337\text{ m}^2\text{ g}^{-1}$ for the Al-D solid, while the largest values of $0.98\text{ cm}^3\text{ g}^{-1}$ for the pore volume and 7.4 nm for the pore diameter are obtained at an intermediate value of P123 content, that is 0.3 mole of P123 added per mol of Al^{3+} (Al-C solid). These results suggest that to preserve a surface area larger than $400\text{ m}^2\text{ g}^{-1}$, the structuring agent content has to be lower than 0.3 mole per mol of Al^{3+} in the studied range.

The isotherm obtained for the solid prepared without porogen Al-A is intermediate between type IV and type II, whereas a pure type IV isotherm is obtained (shown for Al-B, Fig. 1a) for solids prepared with P123. This suggests more homogeneous aggregation of particles in the case of the solid prepared with P123. Pore size distribution also appears larger in the presence of porogen (Al-B) than without (Al-A) (Fig. 1b), while in the literature, in the case of organized mesoporous structures, the presence of the structuring agent usually leads to narrower pore size distributions. For the solids synthesized in this work, porosity seems to be generated by the arrangement of elementary crystallites, the repartition of the pore size being more related to their size and arrangement. No modification of the isotherm shape is further driven by par the porogen content increase. Then, in contrast to what is observed for ordered materials, no formation of channel-type porosity (as in silica materials, e.g. SBA-15, KIT-6, MCM-41) is awaited since porosity originates from elementary particle arrangements in the aggregates formed.

Effect of the quantity of water during the hydrolysis step, B–E–F aluminas in Table 2. The quantity of water added for the hydrolysis step increased from 3.0 to 5.9 mol of H_2O per mol of Al^{3+} : Al-B (3 mol), Al-E (4.5 mol) and Al-F (5.9 mol). A decrease in

Table 2 Textural properties of alumina supports and derived catalysts

Sample	S_{BET} ($\text{m}^2\text{ g}^{-1}$)	V_p ($\text{cm}^3\text{ g}^{-1}$)	D_p (nm)	dMo_{max} (at per nm^2)	S_{BET}^a ($\text{m}^2\text{ g}^{-1}$)	V_p^a ($\text{cm}^3\text{ g}^{-1}$)	D_p (nm)	dMo_{real} (at per nm^2)	ΔS_{BET} (%)	ΔD_p (%)	ΔV_p (%)
Al-A: Al-S0-W3-Th15-HT45 CoMo24.0/Al-A	359	0.62	5.4	4.1	—	—	—	—	—	—	—
Al-B: Al-S0.2-W3-Th15-HT45 CoMo22.8/Al-B	445	0.78	6.0	3.1	331	0.47	4.6	4.3	-8	-15	-24
Al-C: Al-S0.3-W3-Th15-HT45	412	0.98	7.4	—	303	0.55	6.0	4.4	-32	0	-29
Al-D: Al-S0.6-W3-Th15-HT45	337	0.70	6.8	—	—	—	—	—	—	—	—
Al-E: Al-S0.2-W4.5-Th15-HT45 CoMo27.4/Al-E	438	1.26	9.0	5.3	—	—	—	—	—	—	—
Al-F: Al-S0.2-W5.9-Th15-HT45 CoMo25.9/Al-F	402	1.31	8.9	6.3	375	0.81	7.3	4.7	-15	-19	-36
Al-G: Al-S0.2-W3-Th25-HT45	429	1.04	7.5	—	266	0.64	7.2	6.0	-34	-19	-51
Al-H: Al-S0.2-W3-Th50-HT45 CoMo26.1/Al-H	407	1.00	7.6	4.6	—	—	—	—	—	—	—
Al-I: Al-S0.2-W3-Th15-HT15 CoMo21.1/Al-I	402	0.81	6.1	3.3	354	0.76	7.4	4.6	-13	-3	-24
Al-J: Al-S0.2-W3-Th15-HT65	409	0.97	6.5	—	318	0.61	6.0	3.8	-21	-2	-25
Al-K: Al-S0.2-W3-Th15-HT85	407	1.03	7.5	—	—	—	—	—	—	—	—
Al-P: Pural CoMo14.1/Al-P	179	0.46	7.3	4.8	196	0.45	7.3	4.0	-9	0	-2

^a Values corrected by removing the contribution of the weight gain consecutive to the introduction of the active phase (expressed per gram of support).

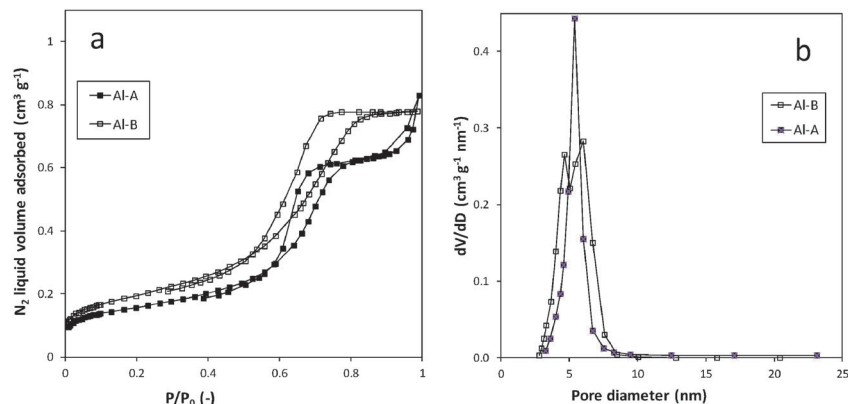


Fig. 1 Effect of adding porogen on the N_2 adsorption–desorption isotherm shape (a) and BJH pore size distributions (b); comparison between Al-A (without porogen) and Al-B.

SSA is observed, from $445 \text{ m}^2 \text{ g}^{-1}$ for sample Al-B to $402 \text{ m}^2 \text{ g}^{-1}$ for sample Al-F, but the three materials present values of SSA above $400 \text{ m}^2 \text{ g}^{-1}$. A significant increase in pore volume and pore diameter is observed with the water content increase, with maximum values of pore volume and pore diameter being $1.31 \text{ cm}^3 \text{ g}^{-1}$ and $\sim 9.0 \text{ nm}$, respectively, obtained for Al-F prepared with the highest water content. A significant modification of the isotherm shape is however observed with the increase in H_2O content used for the hydrolysis step: the isotherm is type IV with 3 moles of H_2O and is shifting to type-IV and II complex isotherms at higher water content (Fig. 2). At the highest water content, the contribution of the type II is becoming predominant.

Hydrolysis temperature effect, B–G–H aluminas in Table 2. The increase in the hydrolysis temperature, from 15°C (Al-B) to 45°C (Al-H), induces the modification of the textural parameters of the final alumina. However, the isotherm shape remains unchanged, pure type IV shape, whatever the hydrolysis temperature in the range considered. The main impact of the hydrolysis temperature is on the surface area that decreases with the increase in hydrolysis temperature. Consequently, decreasing the hydrolysis temperature down to ambient temperature (15°C , for Al-B) allows obtaining a surface area close to $450 \text{ m}^2 \text{ g}^{-1}$. At higher

hydrolysis temperature, the surface area decreases but remains higher than $400 \text{ m}^2 \text{ g}^{-1}$. The decrease in surface area is also accompanied by a slight increase in pore volume and pore volume (Table 2).

Effect of the hydrothermal treatment temperature, I–B–J–K aluminas in Table 2. The temperature applied for the hydrothermal treatment (15°C (Al-I) to 85°C (Al-K)) also impacts the textural properties of the final alumina. All the materials from this series present SSA above $400 \text{ m}^2 \text{ g}^{-1}$, the highest value being obtained at 45°C (Al-B with $445 \text{ m}^2 \text{ g}^{-1}$). While an increase in temperature from 15°C to 45°C does not significantly impact the pore volume and the pore size, both parameters are observed to progressively increase with the hydrothermal treatment from 45°C to 85°C . At 85°C , the pore volume reaches $1.03 \text{ cm}^3 \text{ g}^{-1}$ with a mean pore diameter of 7.5 nm . The increase in hydrothermal temperature does not result in a modification of the isotherm shape that remains of pure type IV whatever the autoclave temperature (type IV, Fig. 3).

From this series of materials, aluminas with different textural properties were selected according to (i) decreasing SSA: Al-B > Al-E > Al-F, Al-H, Al-I > Al-A >> Al-P, and (ii) decreasing pore volume: Al-F > Al-E > Al-H > Al-B, Al-I > Al-A >> Al-P, with Al-F, Al-H, and Al-I at the almost iso-surface area.

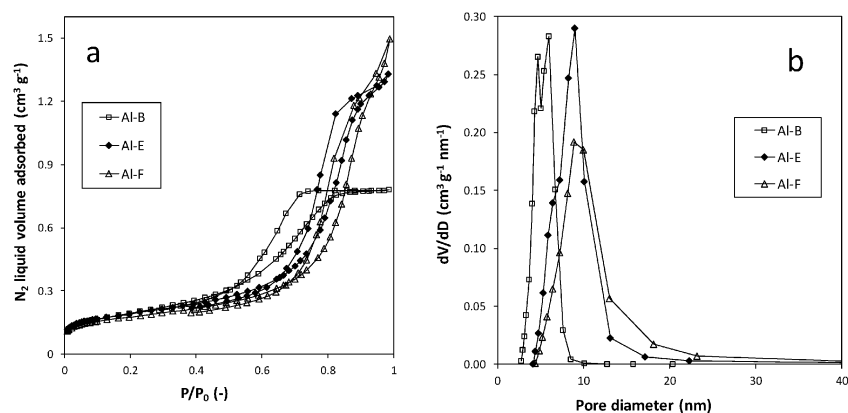


Fig. 2 N_2 adsorption–desorption isotherms (a) and BJH pore size distributions (b) of aluminas Al-B, Al-E and Al-F ($n(H_2O) = 2.9, 4.5, 5.9$).

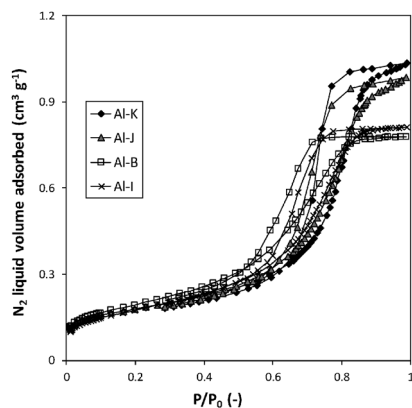


Fig. 3 N_2 adsorption–desorption isotherms obtained for aluminas prepared at different hydrothermal treatment temperatures. Al-I, 15 °C; Al-B, 45 °C; Al-J, 65 °C, and Al-K, 85 °C.

3.2. CoMo oxidic precursor properties

3.2.1 Stability of supports upon impregnation-calcination processes. CoMo oxidic precursors were characterized after impregnation and calcination. All the samples retain isotherms similar to those obtained before impregnation. Indeed, CoMo-containing materials derived from Al-B, Al-H and Al-I present the isotherm of type IV (as shown for catalysts prepared on Al-I in Fig. 4a), whereas Al-A, Al-E and Al-F based ones exhibit a mixed II/IV isotherm shape (as illustrated in Fig. 5a for catalyst CoMo27.4/Al-E).

Significant variations of the textural parameters are observed upon catalyst preparation (Table 2). For CoMo22.8/Al-B, CoMo21.1/Al-I and CoMo25.9/Al-F, a significant decrease in SSA is noticed (larger than 20% of SSA decrease), while for CoMo26.1/Al-H, CoMo27.4/Al-E and CoMo24.0/Al-A, a smaller SSA reduction is measured, with ΔS_{BET} always inferior to 15%. For CoMo22.8/Al-B, CoMo21.1/Al-I and CoMo26.1/Al-H, the pore sizes and pore size distributions remain of comparable value to that of the bare corresponding alumina supports (Fig. 4b and Table 2, decrease of value below 4%). Larger evolutions are observed for catalysts CoMo27.4/Al-E, CoMo25.9/Al-F and CoMo24.0/Al-A, with the decrease in pore size being between 15 and 34%. A significant

decrease in pore volume values is observed for all these materials, larger than 20%, independent of the evolution of the pore diameter and/or surface area. Then, a significant rearrangement of the particles in the aggregates is awaited upon active phase impregnation. The oxidic precursors can be however classified according to the evolution of their textural properties upon impregnation, knowing that the porous volume is always decreasing.

- CoMo26.1/Al-H is the most stable support, with SSA and pore diameter with respective variations of 13% of SSA and 3% of pore diameter.

- CoMo22.8/Al-B and CoMo21.1/Al-I underwent a significant decrease in SSA (32 and 21%) while they retain their pore diameter (variation of 0 and 2%, respectively).

- CoMo27.4/Al-E and CoMo25.9/Al-F exhibit a significant decrease in both SSA and pore diameter, with 14 and 34%, respectively, for the SSA and 19% for the pore diameter.

- CoMo24.0/Al-A underwent an important decrease in the pore diameter (15%) with almost no variation of its SSA (8%).

Most of the solids present molybdenum density close to that expected, except for solids CoMo22.8/Al-B and CoMo25.9/Al-F for which the dMo on the final solid is much higher, in agreement with the significant evolution of the support SSA upon impregnation and calcination steps (above 30%).

The fragility of the sol-gel derived aluminas towards impregnation is then clearly evidenced, especially when compared to the textural properties of a commercial Pural alumina that remain unchanged. The sensitivity of mesoporous alumina supports obtained from the sol-gel route for catalyst preparation conditions was already highlighted in previous studies. On alumina obtained by the hydrolysis of aluminum *sec*-butoxide, in the presence of P123, Bejenaru *et al.*³⁶ measured a decrease of 19% for the surface area and of 47% for the pore volume. Pore size distribution was also observed to significantly evolve, from a bimodal one for alumina to a monomodal one, with a narrower width of pore distribution, for the oxidic precursor. Kaluža *et al.*,³⁴ on alumina prepared by the hydrolysis of aluminum *sec*-butoxide in the presence of a stearic acid type template, also observed significant evolution of the textural properties of calcined alumina upon catalyst preparation.

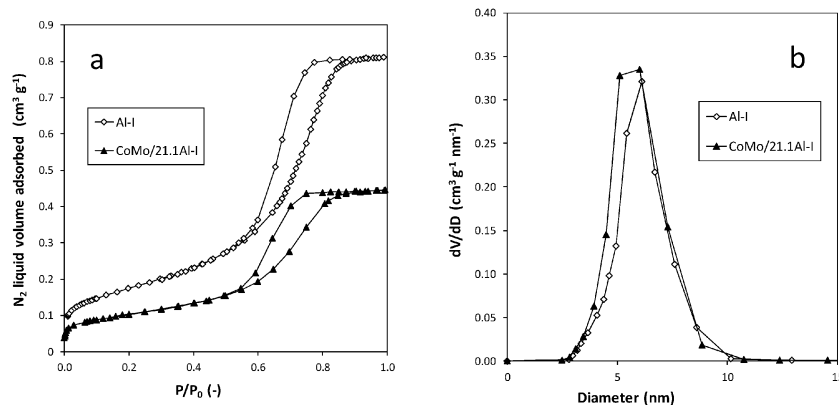


Fig. 4 N_2 adsorption–desorption isotherms (a) and BJH pore size distributions (b) obtained for Al-I and CoMo21.1/Al-I.

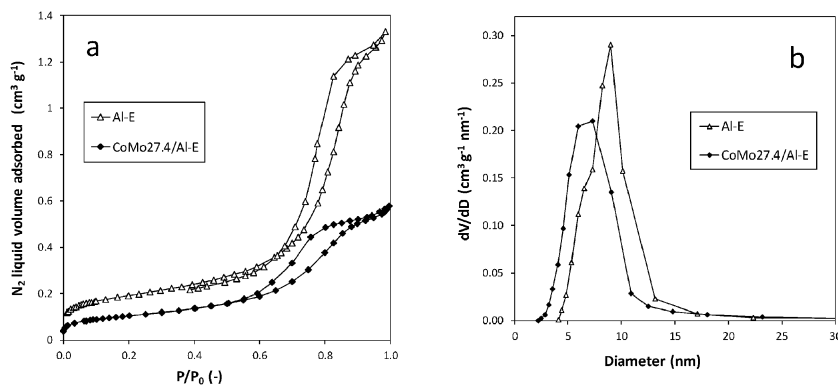


Fig. 5 N₂ adsorption-desorption isotherms (a) and BJH pore size distributions (b) obtained for Al-E and CoMo27.4/Al-E.

The authors attributed these textural property evolutions to a sintering of particles during the thermal treatment step. However, despite significant textural property modifications, final catalysts still present adequate properties for use in the heterogeneous catalysis process. In addition, the use of these mesoporous supports allows increasing the loading in the active phase (up to 27 wt% MoO₃, Table 2), while the loading is limited when classical support, like commercial Pural support (14.1 wt%, Table 2), is used.

3.2.2 Dispersion of cobalt and molybdenum species in the oxidic precursors. Fig. 6 shows the Raman spectra of the CoMo catalysts. Materials can be classified according to the species identified. CoMo22.8/Al-B, CoMo21.1/Al-I and CoMo26.1/Al-H present a broad line at 952 cm⁻¹, corresponding to polymolybdate species well dispersed on the support surface (Fig. 6a), similar to what is observed by impregnation over classical alumina.^{40,41} Lines at 690, 480 and 516 cm⁻¹, attributed to Co₃O₄, are also identified.⁴² While the intensity of the lines associated with polymolybdate species remains unchanged, the intensity of the line at 690 cm⁻¹ is low in the Raman spectra of CoMo21.1/Al-I and CoMo26.1/Al-H catalysts compared to CoMo22.8/Al-B, indicating that Co₃O₄ is probably minor on these two solids. On CoMo27.4/Al-E, CoMo25.9/Al-F and CoMo24.0/Al-A (Fig. 6b), lines identified at 820 and 940 cm⁻¹ evidence the presence of β-CoMoO₄, characteristic of a poor dispersion of molybdenum species in the porous network of the support.⁴³ However considering the very high diffusion cross-section of CoMoO₄ compared to that of polymolybdate species, the presence of well-dispersed polymolybdate species can also be assumed.

Over conventional alumina, Mazurelle *et al.*, with the same impregnating precursor, observed the formation of MoO₃ and CoMoO₄ for a loading largely lower than the one reported in the present study (~16 wt% MoO₃).³⁵ The limited pore volume (0.8 cm³ g⁻¹) displayed by the γ-alumina extrudates used is at the origin of the poor Mo phase dispersion (at a surface density of 4.3 at_{Mo} nm⁻²). Indeed at this Mo loading, considering the support pore volume, the impregnation solution is saturated, leading to precipitation during the impregnation/drying step.

The formation of Co₃O₄ is usually not observed when using the Co₂Mo₁₀ heteropolycompound as a precursor of molybdenum and cobalt, and whatever the support nature (zirconium oxide, titanium oxide or γ-alumina).^{35,43-47} However, commercial supports, classically used for hydrotreatment studies, are highly stable toward the impregnation process.^{43,44}

All sol-gel aluminas of our series underwent a decrease in surface area and pore volume during the impregnation/calcination process. For the three solids CoMo27.4/Al-E, CoMo25.9/Al-F and CoMo24.0/Al-A with CoMoO₄, a severe decrease in pore diameter (between 15 and 19%) is observed in addition to the decrease in pore volume. In our case the concentration of the impregnating solutions is calculated to obtain a dMo inferior to the maximum dMo imposed by the initial water pore volume of the support. Thus the solutions are not saturated and no CoMoO₄ is expected after calcination. But the modification of the porous network during the impregnation step induces an excess of solution outside the pores and subsequent precipitation during the drying step of CoMo species leading to the formation of CoMoO₄ during calcination.

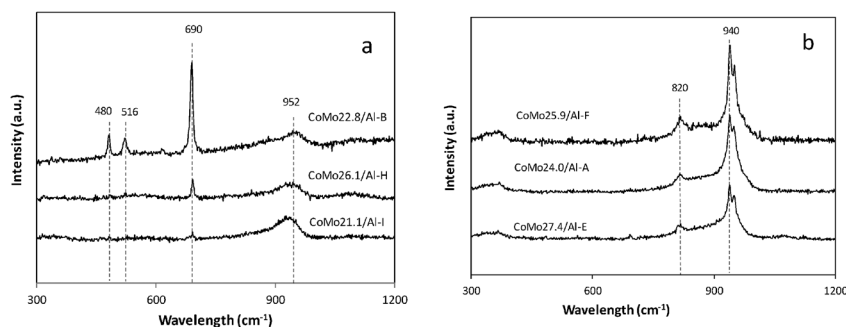


Fig. 6 Raman spectra obtained for the CoMo oxidic precursors.

On the other hand, solids with Co_3O_4 present a stable pore diameter upon impregnation (with limited variations between 0 and 4%). $\text{Co}_2\text{Mo}_{10}$ solution, used for impregnation, exhibits a slightly acidic pH (close to 4). Under these conditions, the alumina surface is positively charged (the alumina zero point charge is ~ 8).⁴⁸ $[\text{Co}_2\text{Mo}_{10}\text{O}_{38}\text{H}_4]^{6-}$ anions are expected to interact with the positively charged surface of alumina. However, free Co^{2+} counter cations in solution will not interact with the surface support. It seems that in the case of the decrease in porous volume while maintaining the pore diameter, a significant amount of Co^{2+} containing solution can be expelled outside the pores and precipitates as Co hydroxide out of the internal porosity during the solvent evaporation step, leading to the formation of Co_3O_4 upon thermal treatment. In any case, molybdenum species are well dispersed in these solids, demonstrating the ability of these sol-gel supports to maintain high molybdenum dispersion at high Mo content (up to 26.1 wt% MoO_3).

3.2.3 Surface analysis of the oxidic precursors. XPS spectra of Al2p, O1s, Mo3d, Co2p and C1s levels were recorded. Fig. 7 shows the typical spectra of Mo3d and Co2p levels, recorded for CoMo26.1/Al-H. For all materials, the Mo3d_{5/2} and Co2p_{3/2} photopeaks are located at binding energies of 233.1 ± 0.2 eV and 781.5 ± 0.2 eV, respectively. These positions are characteristic of Mo^{6+} and Co^{2+} species in oxidic environments.

Table 3 presents atomic surface ratios, as determined by XPS, as well as theoretical bulk ratios. For all solids, $n_{\text{Mo}}/n_{\text{Al}}$ surface ratios are higher than the bulk ones, the differences being independent of the presence or not of CoMoO_4 . Indeed, the CoMoO_4 phase should lead to lower surface ratios than bulk ratios, as only a fraction of molybdenum is detected in these bulk particles.⁴⁹ This difference can be due to the presence in our case of particles of CoMoO_4 small enough to ensure the complete detection of molybdenum by XPS, and/or to large alumina particles with consequently not all Al atoms detected by XPS. Concerning $n_{\text{Co}}/n_{\text{Al}}$ surface ratios, values appear to be lower than bulk ratios, except for sample CoMo21.1/Al-I (increase of 12%) that contains a low quantity of Co_3O_4 compared to other samples. Obtaining a lower $n_{\text{Co}}/n_{\text{Al}}$ surface ratio could thus be due to the presence of Co_3O_4 or CoMoO_4 . These lower ratios could also be related to the migration of cobalt atoms in the tetrahedral sites of alumina particles that would be too large to be completely analyzed by XPS.

Table 3 $n_{\text{Mo}}/n_{\text{Al}}$, $n_{\text{Co}}/n_{\text{Al}}$ and $n_{\text{Co}}/n_{\text{Mo}}$ atomic ratios; (th) theoretical values calculated from material composition; (XPS) experimental values obtained from XPS analysis

Sample	$n_{\text{Mo}}/n_{\text{Al}}$ (th)	$n_{\text{Mo}}/n_{\text{Al}}$ (XPS)	$n_{\text{Co}}/n_{\text{Al}}$ (th)	$n_{\text{Co}}/n_{\text{Al}}$ (XPS)	$n_{\text{Co}}/n_{\text{Mo}}$ (XPS)	C _{1s} (%)
CoMo24.0/Al-A	0.12	0.16	0.061	0.050	0.31	0.8
CoMo22.8/Al-B	0.11	0.13	0.057	0.054	0.42	11.1
CoMo27.4/Al-E	0.15	0.17	0.074	0.051	0.30	18.3
CoMo25.9/Al-F	0.14	0.19	0.068	0.050	0.27	19.6
CoMo26.1/Al-H	0.14	0.15	0.069	0.054	0.37	17.4
CoMo21.1/Al-I	0.10	0.14	0.051	0.057	0.40	8.5

The values of $n_{\text{Co}}/n_{\text{Mo}}$ ratios are all lower than the theoretical value of 0.5. The highest ratios are obtained for the Co_3O_4 containing solids, with values around 0.4, close to the optimum Co/Mo ratio of 0.5 as reported in the literature.⁴¹

Finally, all materials exhibit a high surface carbon content, ranging between 8 and 19% (Table 3), except for catalyst CoMo24.0/Al-A, prepared without a porogen, presenting a very low percentage (0.8%). This indicates that the carbon deposition observed in the other solids is mainly related as expected to the carbon residues issued from the calcination of the structuring agent.

3.3. Catalytic performances in the HDS of thiophene

Catalytic performance of the solids was evaluated in the HDS of thiophene at 300 °C (Table 4). Reaction rates are found to vary over a wide range, from 79.3 to 209.4 $\text{L h}^{-1} \text{kg}^{-1}$, depending on the support used. CoMo24.0/Al-A presents the lowest reaction rate, of only 79.3 $\text{L h}^{-1} \text{kg}^{-1}$, and CoMo26.1/Al-H is the most active material from the series, with a reaction rate of 209.4 $\text{L h}^{-1} \text{kg}^{-1}$. Meanwhile, CoMo22.8/Al-B, CoMo21.1/Al-I, CoMo27.4/Al-E and CoMo25.9/Al-F present intermediate reaction rates, in a narrow range between 133.1 and 147.1 $\text{L h}^{-1} \text{kg}^{-1}$. For these materials, the molybdenum loading varies between 21 and 27% and despite these significant differences in Mo loading, they present similar activities. Under comparable reaction conditions, Bejenaru *et al.*³⁶ reported variable activities, between 55.1 and 161.1 $\text{L h}^{-1} \text{kg}^{-1}$, for CoMo-S materials with 10 wt% Mo, issued from the impregnation of mesostructured aluminas with different morphologies with conventional precursors *i.e.* ammonium heptamolybdate and cobalt nitrate.

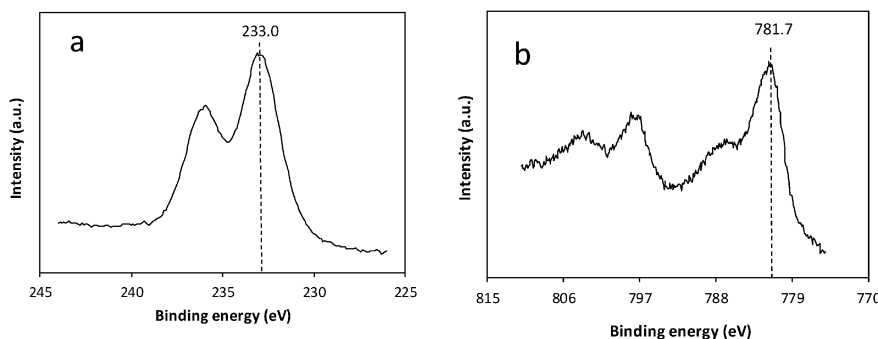


Fig. 7 XPS spectra of Mo3d (a) and Co2p (b) levels recorded for CoMo26.1/Al-H.

Table 4 Catalytic properties of the synthesized materials in the thiophene HDS reaction at 300 °C. Reaction rates are expressed per kg of catalyst or normalized per mole of molybdenum

Sample	Reaction rate (L h ⁻¹ kg ⁻¹)	Normalized reaction rate (L h ⁻¹ mol _{Mo} ⁻¹)
CoMo24.0/Al-A	79.3	47.6
CoMo22.8/Al-B	145.9	92.1
CoMo27.4/Al-E	133.1	70.0
CoMo25.9/Al-F	147.1	81.8
CoMo26.1/Al-H	209.4	115.5
CoMo21.1/Al-I	135.3	92.3
CoMo14.1/Al-P	153.5	156.1

Activities reported here are significantly higher, but the materials prepared in this study present higher Mo loadings (Table 2). The CoMo catalyst prepared over commercial Pural alumina also shows an intermediate activity of 153.5 L h⁻¹ kg⁻¹, an activity coherent with those reported in the literature for commercial alumina supported CoMo catalysts. Indeed, Glasson *et al.*⁵⁰ measured the reaction rate in thiophene HDS at 300 °C around 141 L h⁻¹ kg⁻¹ for a CoMo catalyst supported on commercial alumina (12.3% Mo). Materials presented here appear therefore to be particularly efficient, especially considering CoMo26.1/Al-H with activity at least 20% higher than those reported in the literature.

In order to compare the performance of solids at different Mo loadings, reaction rates were normalized per mole of molybdenum. Normalized activity is found to vary also by a factor 3, between 47.6 and 115.5 L h⁻¹ mol_{Mo}⁻¹. The most efficient solid, CoMo26.1/Al-H, is the material prepared with the support presenting the best stability toward impregnation: the modification of SSA of 13% and the pore diameter of only 3%. CoMo22.8/Al-B and CoMo21.1/Al-I present a lower and comparable normalized reaction rate (92 L h⁻¹ mol_{Mo}⁻¹) for similar final SSA (~300 m² g⁻¹). However, both supports suffered from the significant porous volume decrease upon impregnation while the pore diameter remained unchanged. These three solids, CoMo22.8/Al-B, CoMo21.1/Al-I and CoMo26.1/Al-H, present similar pore characteristics (type IV isotherms) and well-dispersed polymolybdate species as evidenced by Raman spectroscopy. The presence of Co₃O₄ is evidenced in these three solids, suggesting that the loss of a fraction of the initial cobalt in the form of a poorly dispersed bulk oxide phase (that will not incorporate the CoMoS active phase) does not directly influence the material catalytic performance. This result can be explained on the basis of literature data analysis. Indeed, theoretical calculations, based on the density functional theory (DFT), showed that a ratio Co/Mo of 0.3 is enough to promote in an optimal way the MoS₂ slabs.^{51,52} Consequently, the loss of part of cobalt in the form of bulk cobalt oxide, in the case of the Al-B, Al-H and Al-I supports, does not significantly impact the activity of the catalysts since sufficient well dispersed cobalt atoms remain for promoting the MoS₂ slabs, these three solids presenting the highest Co/Mo XPS atomic ratio (around 0.4). It can also be noted that for these three solids, the amount of residual carbon content is relatively high (around 18%) and could thus impact catalytic activity. Indeed the presence of

residual carbon has been reported to be beneficial by several authors that suggest that carbon may induce different sulfidation degrees of Co and Mo, and different structures and/or morphologies of the generated active phase.^{53,54} Different sulfidation degrees of Mo and Co may obviously lead to more or less promoted and dispersed active phases.⁵⁵ The role of carbonaceous residues of the support surface in the sulfided phase properties is multiple. Heat generated by the sulfidation reaction can be partially absorbed by these residues, resulting in crystallite growth different from that over carbon free support.⁵⁰ Glasson *et al.*⁵⁰ observed positive effects of the presence of carbonaceous species on the CoMo-S/Al₂O₃ activity for the HDS of thiophene and petroleum fractions. These authors also stated that carbon restricts or inhibits the migration and/or growth of the sulfided phase, isolating active phase crystallites (geometric order effect). Also, Co(Ni)Mo-S supported over activated carbon showed higher HDS activity than the active phase supported on alumina.⁵⁶⁻⁵⁹ The formation of an active carbide phase, “CoMoC”, could also explain the better performance when the active phase is supported over carbon.⁶⁰ Consequently, such a phenomenon, modifying the intrinsic activities of the CoMo-S phase, could not be excluded over these carbon containing supports.

On CoMo27.4/Al-E and CoMo25.9/Al-F, intermediate activities at around 70–80 L h⁻¹ mol_{Mo}⁻¹ are obtained. These supports present low stability upon impregnation, with a significant decrease in both SSA (14 and 34%) and pore diameter (19%). Raman spectroscopy evidenced the formation of CoMoO₄ species, which can explain the lower performances of these solids. Consequently, if the supports were stabilized before impregnation, significantly higher activity could be achieved since the pore network reorganization is expected to be at the origin of the formation of this detrimental CoMoO₄ phase. Finally, the lowest performance is obtained for CoMo24.0/Al-A (47.6 L h⁻¹ mol_{Mo}⁻¹), which can be related to both the detrimental presence of CoMoO₄ species and to the lowest carbon content (0.8%) since the parent support is prepared without an organic porogen. The catalyst CoMo14.1/Al-P prepared on the commercial alumina presents the highest conversion per mole of molybdenum (156.1 L h⁻¹ mol_{Mo}⁻¹). However higher conversion per mass of catalyst could be achieved for derived sol-gel alumina based solids since their textural properties allow higher molybdenum loading, while preserving satisfying molybdenum dispersion.

3.4. Catalytic performances in the HDS of SRGO

The most efficient catalyst in the HDS of thiophene CoMo28.7/Al-H was selected for further evaluation of its performance in the HDS of a SRGO, to be compared to that of the commercial Pural based solid. For both solids, the residual sulfur content in the hydrotreated product is plotted as a function of the reactor temperature, as shown in Fig. 8. The mesoporous sol-gel based catalyst appears to be significantly more efficient than the commercial supported one (per volume of catalyst and per mass of catalyst, taking into account their similar apparent densities), with 74 *versus* 415 ppmS at 350 °C and 10 *versus* 100 ppmS at 370 °C. Moreover, these performances are close to that of a

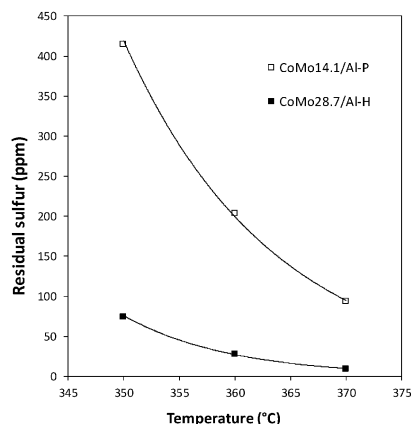


Fig. 8 Catalytic performance of the CoMo28.7/Al-H and CoMo14.1/Al-P catalysts in the HDS of a SRGO: residual sulfur content in the desulfurized feed versus the temperature of the reactor.

commercial catalyst modified by a chelating agent, evaluated under the same conditions.⁶¹

These results clearly evidence the potential of the sol-gel aluminas developed in this study as support for the HDS catalyst, not only in the conversion of model molecules but more interestingly also in the desulfurization of real feedstocks. From our knowledge, this is the first time a mesoporous sol-gel alumina based CoMo HDS catalyst was evaluated in HDS of SRGO under experimental conditions representative of industrial ones.

4. Conclusions

Alumina supports were prepared using a template assisted sol-gel method. The adjustment of alumina textural properties was performed through the control of synthesis parameters, such as the quantity of porogen, the quantity of water, the temperature of the hydrolysis step, and the temperature of the hydrothermal treatment. High surface areas, close to 400 m² g⁻¹ for most of the aluminas, were obtained with pore diameters up to 9 nm. Among the prepared materials, six supports, with varying textural properties, were selected for the preparation of CoMo-S HDS catalysts.

Characterization revealed a fragility of the support texture toward the impregnation. A significant decrease in surface area, pore volume and pore diameter is observed depending on the materials. However, despite these significant alterations, the final values of textural parameters remain attractive for HDS catalyst preparation. Characterization of the oxidic precursors evidenced two groups of solids, one where molybdenum species are well dispersed on the support (over the more stable supports), and the other where the presence of β -CoMoO₄ is observed (the more sensible supports, the formation of this phase being related to the pore diameter decrease during the impregnation process). The performance in thiophene HDS at 300 °C varies by a factor 3 depending on the support used. Low activity is measured for materials showing the formation of a CoMoO₄ phase before sulfidation. Higher activity is measured over the more stable supports, the most efficient solid of the series showing the best stability toward impregnation. These materials are less active

than a catalyst prepared over commercial alumina, when comparing the activity normalized per molybdenum atom. However, the use of these supports allows us to reach higher activities per gram of catalyst, due to the possibility of significantly increasing the Mo loading without the formation of detrimental phases (CoMoO₄).

The most efficient catalyst in the HDS of thiophene, CoMo28.7/Al-H, was evaluated in the HDS of a SRGO. Its performance appears to be higher than that of the commercial Pural based catalyst and close to that of a commercial catalyst modified by a chelating agent, evaluated under the same conditions.

These results clearly evidence the potential of the sol-gel aluminas developed in this study as support for a highly loaded HDS catalyst, not only in the conversion of model molecules but also more interestingly in the desulfurization of real feedstocks, with the challenge now to stabilize the porosity of these supports.

Acknowledgements

The Equatorial Government (for the attribution of a PhD grant to A. Miño) and IFPEN (for financial support) are acknowledged. Chevrel Institute (FR 2638), Ministère de l'Enseignement Supérieur et de la Recherche, Région Nord – Pas de Calais and FEDER are acknowledged for supporting and funding this work. M. Trentesaux is acknowledged for XPS analysis support.

References

- 1 Directive 2009/30/EC of the European Parliament.
- 2 H. Topsøe, B. S. Clausen and F. E. Massoth, *Hydrotreating Catalysis*, Springer, Berlin, 1996.
- 3 R. Prins, V. H. J. De Beer and G. A. Somorjai, *Catal. Rev.: Sci. Eng.*, 1989, **32**, 1.
- 4 E. J. M. Hensen, Y. van der Meer, J. A. R. van Veen and J. W. Niemantsverdriet, *Appl. Catal., A*, 2007, **322**, 16.
- 5 J. F. Lepage, *Catalyse de Contact: conception, préparation et mise en œuvre des catalyseurs industriels*, TECHNIP, Paris, 1978.
- 6 S. Dzwigaj, C. Louis, M. Breyse, M. Cattenot, V. Bellière, C. Geantet, M. Vrinat, P. Blanchard, E. Payen, S. Inoue, H. Kudo and Y. Yoshimura, *Appl. Catal., B*, 2003, **41**, 181.
- 7 C. Lamonier, D. Soogund, J. Mazurelle, P. Blanchard, D. Guillaume and E. Payen, *Stud. Surf. Sci. Catal.*, 2006, **162**, 713.
- 8 I. Merdignac and D. Espinat, *Oil Gas Sci. Technol.*, 2007, **62**, 7.
- 9 C. T. Kresge, M. E. Leonowicz, W. J. Roth, J. C. Vartuli and J. S. Beck, *Nature*, 1992, **359**, 710.
- 10 S. A. Bagshaw and T. J. Pinnavaia, *Angew. Chem.*, 1996, **35**, 1102.
- 11 F. Vaudry, S. Khodabandeh and M. E. Davis, *Chem. Mater.*, 1996, **8**, 1451.
- 12 S. Valange, J.-L. Guth, F. Kolenda, S. Lacombe and Z. Gabelica, *Microporous Mesoporous Mater.*, 2000, **35–36**, 597.
- 13 C. Márquez-Alvarez, N. Žilková, J. Pérez-Pariente and J. Čejka, *Catal. Rev.: Sci. Eng.*, 2008, **50**, 222.

- 14 K. Niesz, P. Yang and G. A. Somorjai, *Chem. Commun.*, 2005, 1986.
- 15 Q. Yuan, A.-X. Yin, C. Luo, L.-D. Sun, Y.-W. Zhang, W.-T. Duan, H.-C. Liu and C.-H. Yan, *J. Am. Chem. Soc.*, 2008, **130**, 3465.
- 16 J.-P. Dacquain, J. Dhainaut, D. Duprez, S. Royer, A. F. Lee and K. Wilson, *J. Am. Chem. Soc.*, 2009, **131**, 12896.
- 17 W. Zhang and T. J. Pinnavaia, *Chem. Commun.*, 1998, 1185.
- 18 T. J. Pinnavaia, Z. Zhang and R. W. Hicks, *Stud. Surf. Sci. Catal.*, 2005, **156**, 1.
- 19 J. Čejka, P. J. Kooyman, L. Veselá, J. Rathouský and A. Zúkal, *Phys. Chem. Chem. Phys.*, 2002, **4**, 4823.
- 20 K. Niesz, P. Yang and G. A. Somorjai, *Chem. Commun.*, 2005, 1986.
- 21 A. Caragheorghieopol, H. Calderaru, G. Ionita, F. Savonea, N. Žilková, A. Zúkal and J. Čejka, *Langmuir*, 2005, **21**, 2591.
- 22 L. Vradman, M. V. Landau, M. Herskowitz, V. Ezersky, M. Taliander, S. Nikitenko, Y. Koltypin and A. Gedanken, *J. Catal.*, 2003, **213**, 163.
- 23 L. Lizama and T. Klimova, *Appl. Catal., B*, 2008, **82**, 139.
- 24 R. Huirache-Acuna, B. Pawelec, E. Rivera-Munoz, R. Nava, J. Espino and J. L. G. Fierro, *Appl. Catal., B*, 2009, **92**, 168.
- 25 V. La Parola, B. Dragoi, A. Ungureanu, E. Dumitriu and A. M. Vanezia, *Appl. Catal., A*, 2010, **386**, 43.
- 26 P. E. Boahene, K. K. Soni, A. K. Dalai and J. Adjaye, *Appl. Catal., A*, 2011, **402**, 31.
- 27 T. Chiranjeevi, G. Muthu Kumaran and G. Murali Dhar, *Pet. Sci. Technol.*, 2008, **26**, 690.
- 28 M. Hussain, S.-K. Song, J.-H. Lee and S.-K. Ihm, *Ind. Eng. Chem. Res.*, 2006, **45**, 536.
- 29 R. Nava, A. Infantes-Molina, P. Castao, R. Guil-Lopez and B. Pawelec, *Fuel*, 2011, **90**, 2726.
- 30 T. A. Zepeda, T. Halachev, B. Pawelec, R. Nava, T. Klimova, G. A. Fuentes and J. L. G. Fierro, *Catal. Commun.*, 2006, **7**, 33.
- 31 K. Soni, K. C. Mouli, A. K. Dalai and J. Adjaye, *Catal. Lett.*, 2010, **136**, 116.
- 32 M. T. Nguyen Dinh, P. Rajbhandari, C. Lancelot, P. Blanchard, C. Lamonier, M. Bonne, S. Royer, F. Dumeignil and E. Payen, *ChemCatChem*, 2014, **6**, 328.
- 33 J. Čejka, N. Žilková, L. Kaluža and M. Zdražil, *Stud. Surf. Sci. Catal.*, 2002, **141**, 243.
- 34 L. Kaluža, M. Zdražil, N. Žilková and J. Čejka, *Catal. Commun.*, 2002, **3**, 151.
- 35 J. Mazurelle, C. Lamonier, C. Lancelot, E. Payen, C. Pichon and D. Guillaume, *Catal. Today*, 2008, **130**, 41.
- 36 N. Bejenaru, C. Lancelot, P. Blanchard, C. Lamonier, L. Rouleau, E. Payen, F. Dumeignil and S. Royer, *Chem. Mater.*, 2009, **21**, 522.
- 37 S. Badoga, R. V. Sharma, A. K. Dalai and J. Adjaye, *Appl. Catal., A*, 2015, **489**, 86.
- 38 C. Martin, C. Lamonier, M. Fournier, O. Mentré, V. Harlé, D. Guillaume and E. Payen, *Chem. Mater.*, 2005, **17**, 4438.
- 39 M. J. Ledoux, C. P. Huu and F. Luck, *J. Catal.*, 1990, **121**, 70.
- 40 E. Payen, J. Grimblot, J. C. Lavalley, M. Daturi and F. Maugé, *Handbook of Vibrational Spectroscopy*, John Wiley & Sons, 2006.
- 41 P. Blanchard, C. Lamonier, A. Griboval and E. Payen, *Appl. Catal., A*, 2007, **322**, 33.
- 42 C.-W. Tang, C.-B. Wang and S.-H. Chien, *Thermochim. Acta*, 2008, **473**, 68.
- 43 C. Lamonier, C. Martin, J. Mazurelle, V. Harlé, D. Guillaume and E. Payen, *Appl. Catal., B*, 2007, **70**, 548.
- 44 C. I. Cabello, F. M. Cabrerizo, A. Alvarez and H. J. Thomas, *J. Mol. Catal. A: Chem.*, 2002, **166**, 89.
- 45 P. A. Nikulshin, D. I. Ishutenko, A. A. Mozhaev, K. I. Maslakov and A. A. Pimerzin, *J. Catal.*, 2014, **312**, 152.
- 46 P. A. Nikulshin, A. V. Mozhaev, K. I. Maslakov, A. A. Pimerzin and V. M. Kogan, *Appl. Catal., B*, 2014, **158-159**, 161.
- 47 Al. A. Pimerzin, P. A. Nikulshin, A. V. Mozhaev, A. A. Pimerzin and A. I. Lyashenko, *Appl. Catal., B*, 2015, **168-169**, 396.
- 48 P. Euzen, P. Raybaud, X. Krokidis, H. Toulhoat, J.-L. Le Loarer, J. P. Jolivet and C. Froidefond, *Alumina. In Handbook of Porous Solids*, Wiley-VCH, Weinheim, 2002, p. 1591.
- 49 P. Blanchard, E. Payen, J. Grimblot, O. Poulet and R. Loutaty, *Stud. Surf. Sci. Catal.*, 1997, **106**, 211.
- 50 C. Glasson, C. Geantet, M. Lacroix, F. Labruyere and P. Dufresne, *J. Catal.*, 2002, **212**, 76.
- 51 P. Raybaud, J. Hafner, G. Kresse, S. Kasztelan and H. Toulhoat, *J. Catal.*, 2000, **190**, 128.
- 52 A. D. Gandubert, E. Krebs, C. Legens, D. Costa, D. Guillaume and P. Raybaud, *Catal. Today*, 2008, **130**, 149.
- 53 F. Labruyère, P. Dufresne, M. Lacroix and M. Breyse, *Catal. Today*, 1998, **43**, 111.
- 54 J. Vangestel, J. Leglise and J. C. Duchet, *J. Catal.*, 1994, **145**, 429.
- 55 L. Coulier, V. H. J. De Beer, J. A. R. Van Veen and J. W. Niemantsverdriet, *J. Catal.*, 2001, **197**, 26.
- 56 M. Kouzu, Y. Kuriki, F. Hamdy, K. Sakanishi, Y. Sugimoto and I. Saito, *Appl. Catal., A*, 2004, **265**, 61.
- 57 L. Kaluža and M. Zdražil, *Carbon*, 2001, **39**, 2023.
- 58 S. J. Moon and S. K. Ihm, *Korean J. Chem. Eng.*, 1994, **11**, 111.
- 59 E. J. M. Hensen, M. J. Vissenberg, V. H. J. de Beer, J. A. R. van Veen and R. A. van Santen, *J. Catal.*, 1996, **163**, 429.
- 60 R. R. Chianelli and G. Berhault, *Catal. Today*, 1999, **53**, 357.
- 61 N. Frizi, P. Blanchard, E. Payen, P. Baranek, C. Lancelot, M. Rebeilleau, C. Dupuy and J.-P. Dath, *Catal. Today*, 2008, **130**, 32.